Journal of Magnetic Resonance 305 (2019) 16–21

Contents lists available at ScienceDirect

Journal of Magnetic Resonance

journal homepage: www.elsevier.com/locate/jmr

MR-based wall shear stress measurements in fully developed turbulent flow using the Clauser plot method ☆

Nina Shokina [a,*], Andreas Bauer [b], Gabriel Teschner [c], Waltraud B. Buchenberg [a], Cameron Tropea [b], Herbert Egger [c], Jürgen Hennig [a], Axel J. Krafft [a]

[a] Dept. of Radiology, Medical Physics, Medical Center – University of Freiburg, Faculty of Medicine, University of Freiburg, Germany
[b] Institute for Fluid Mechanics and Aerodynamics, Department of Mechanical Engineering, Technische Universität Darmstadt, Darmstadt, Germany
[c] Institute for Numerical Analysis and Scientific Computing, Department of Mathematics, Technische Universität Darmstadt, Darmstadt, Germany

ARTICLE INFO

Article history:
Received 12 April 2019
Revised 21 May 2019
Accepted 24 May 2019
Available online 24 May 2019

Keywords:
Phase-contrast MRI
Wall shear stress
Flow MRI
MR velocimetry
Clauser plot method

ABSTRACT

In arterial blood flow wall shear stress (WSS) quantifies the frictional force that flowing blood exerts on a vessel wall. WSS can be directly estimated from phase-contrast (PC) MR velocity measurements and has been suggested as a biomarker in cardio-vascular diseases. We present and investigate the application of the Clauser plot method for estimating WSS in fully developed turbulent stationary flow using PC velocity measurements. The Clauser plot method estimates WSS from the logarithmic region of boundary layer in fully developed turbulent stationary flow. The Clauser plot method was evaluated using 2D PC-MR phantom measurements at 3 T for different in-plane resolutions at various Reynolds numbers. WSS values derived from the Clauser plot were compared to results from Laser Doppler Velocimetry (LDV) measurements and theoretical results calculated using the friction factor formula for smooth pipe flow. For all Reynolds numbers, WSS values derived from the Clauser plot were in good agreement with results from LDV measurements and values using the friction factor formula (relative deviations ~5%). Furthermore, Clauser plot derived results were almost independent of spatial resolution, in contrast to WSS results obtained with our in-house software tool for MR-based WSS quantification showing relative deviations of more than 100%. In fully developed turbulent flow, the Clauser plot method provides highly consistent WSS independent of the underlying spatial resolution. Therefore, it renders a valuable approach for MR-based WSS estimates in controllable flow settings. Although its direct *in vivo* applicability is severely limited because of the different flow character, it may serve as helpful approach for validation of MR-based WSS quantification algorithms prior to their clinical application.

1. Introduction

In arterial blood flow wall shear stress (WSS) [1] quantifies the frictional force that flowing blood exerts on a vessel wall. The WSS can be directly estimated from phase-contrast (PC) MR velocity measurements [2–10] and has been suggested as a biomarker in cardio-vascular diseases [1,6,11–18].

A direct WSS quantification requires identification of the flow domain, especially its boundary, and computation of the derivative of the velocity field ∇v at the boundary. It has been shown that the accuracy of MR-based WSS values depends strongly on the PC-MR acquisition parameters, the accuracy of the numerical computation of ∇v, and the accuracy of the boundary identification [3,4,8,19,20]. The exact position of the vessel wall is per-se unknown, especially in situations when the vessel wall is moving because of pulsation. Here, even small errors in the boundary identification influence the WSS estimate strongly, because of the transitional flow regime and steep velocity gradients at the boundary.

The main factor for the variability of PC-MR-derived WSS is the limited spatial resolution of the acquired data [3,4,8,19–21]. Partial volume effects act as a main confounder to accurately measure flow velocities in the proximity of the vessel's boundary. Further, the velocities close to the boundary are smaller than the velocities occurring further inside the vessel, so that they more prone to phase noise because the velocity encoding (VENC) parameter is typically chosen according to the expected maximum velocities to avoid phase aliasing [3]. On the other hand, the temporal reso-

☆ Parts of this study were presented at the 26th Annual Meeting of the ISMRM, Paris, France, 2018 (abstract number: 2946).

* Corresponding author at: Medical Center – University of Freiburg, Dept. of Radiology, Medical Physics, Killianstr. 5a, 79106 Freiburg, Germany.
E-mail address: nina.shokina@uniklinik-freiburg.de (N. Shokina).

https://doi.org/10.1016/j.jmr.2019.05.009
1090-7807/

lution of the PC-MR data was shown to have only minor impact on the WSS estimate [3,19].

In vivo comparison against current gold standard methods is problematic for many areas of 4D flow MRI, mostly because of the lack of such a standard *in vivo* [20]. Also, reference data is often not available. For areas where an *in vivo* gold standard does not exist, controlled steady and pulsatile flow phantom experiments with accurate reference quantification can be used to assess WSS accuracy [20].

In this study, we present and investigate the application of the Clauser plot method [22] for WSS quantification to PC-MRI measurement data in a controlled flow setting. The Clauser plot method is a graphical method [22] to estimate WSS within the logarithmic region [23] of the boundary layer in fully developed turbulent stationary flow. It can be applied even in situations when the velocity measurement does not provide sufficient spatial resolution to resolve velocities close to the flow boundary. We describe the Clauser plot method and present its experimental validation in the context of 2D PC-MRI in stationary flows.

2. Theory

Although blood is a shear-thinning non-Newtonian fluid [24], it behaves like a Newtonian fluid with a constant viscosity in larger arteries at high shear rates [25]. This enables calculation of the WSS (τ_w) from the velocity derivative with respect to the normal distance r from the wall:

$$\tau_w = \mu\left(\frac{\partial U(r)}{\partial r}\right)\Big|_{r=0} \tag{1}$$

Here, μ is the dynamic viscosity, and $U(r)$ is the mean streamwise velocity component [8].

Eq. (1) is the most commonly used approach for MR-derived WSS extraction. In contrast, the Clauser plot method evaluates WSS within the logarithmic region of the boundary layer [23]. In the logarithmic region of the boundary layer, the velocity profile $U(r)$ of a fully developed turbulent stationary flow satisfies the logarithmic law

$$\frac{U(r)}{u_\tau} = \frac{1}{\kappa} ln \frac{r u_\tau}{\nu} + B \tag{2}$$

with the shear velocity defined as

$$u_\tau = \sqrt{\frac{\tau_w}{\rho}} \tag{3}$$

Here, ρ indicates density, ν kinematic viscosity ($\nu = \mu/\rho$), and κ and B are constants [26]. The ranges of the constants κ and B are stated in the literature as $\kappa \in [0.33; 0.45]$ [27–29] and $B \in [3.5, 6.15]$ [29]. In our work, to determine the constants κ and B, we fit the law of the wall (2) to a velocity profile obtained by a Direct Numerical Simulation (DNS) of a flow regime [30], that is similar to our setting, yielding $\kappa = 0.3557$ and $B = 4.8175$.

Expressing the wall shear stress in dimensionless form using the skin friction coefficient C_f

$$C_f = 2\left(\frac{u_\tau}{U_\infty}\right)^2 = 2\frac{\tau_w}{U_\infty^2 \rho} \tag{4}$$

Eq. (2) can be expressed as [31]:

$$\frac{U(r)}{U_\infty} = \left[\frac{1}{\kappa}\sqrt{\frac{C_f}{2}}\right] \ln\left(\frac{r U_\infty}{\nu}\right) + \left[\frac{1}{\kappa}\sqrt{\frac{C_f}{2}} \cdot \ln\left(\sqrt{\frac{C_f}{2}}\right) + B\sqrt{\frac{C_f}{2}}\right] \tag{5}$$

known as the Clauser plot equation. Here, U_∞ indicates the free stream velocity outside of the boundary layer, which is known from the measurements. Because ν, κ, and B are known values, only C_f in Eq. (5) is unknown. If $\frac{U(r)}{U_\infty}$ is plotted against $\frac{rU_\infty}{\nu}$ in a semi-log representation for different values of C_f, a set of straight lines is produced. In the original presentation of the Clauser plot method [22], the measured values $\frac{U_{meas}(r)}{U_{\infty,meas}}$ were added to the same graph, and an estimate of C_f, and thus of τ_w, was obtained by visual inspection to choose the line which best reproduced the data within the logarithmic region. Here, we perform a nonlinear regression of the measured data within the logarithmic region to obtain C_f. Then, Eq. (4) is used to compute τ_w instead of using a graphical inspection.

3. Methods

The Clauser plot method for WSS estimation was tested on 2D PC-MR velocity measurements carried out in a glass pipe (inner diameter: 25.9 mm). The pipe was placed inside a 3T whole-body scanner (MAGNETOM Prisma, Siemens Healthineers, Erlangen, Germany) along the magnet's center line, and a turbulent stationary flow was established at a Reynolds numbers of Re = 3000, 5370, 8060. The flow pump (RMMS1, Sondermann, Köln, Germany) was located outside the MR scanner cabin and connected via plastic hoses and straight in-flow pipes (approximate length: 2 m) to ensure fully developed flow conditions. Pure water at room temperature doped with copper sulfate (1 g per liter) [32] was used as a fluid. Our 2D PC-MR technique was a conventional phase-contrast MRI sequence which is based on a spoiled 2D gradient echo sequence with bipolar velocity encoding along the slice selection direction. 2D PC-MR images were acquired in a plane oriented perpendicular to the pipe axis (i.e. axial slice orientation; Fig. 1a) for different in-plane resolutions (range: 0.30 × 0.30–1.00 × 1.00 mm^2) with velocity encoding along the through-plane direction (VENC = 0.25 m/s was chosen for all Reynolds numbers in order to better resolve the velocities close to the vessel boundary). Other scan parameters were as follows: TR/TE = 17.8–18.6/5.66–5.68 ms, FOV = 96 × 96 mm^2, slice thickness = 3 mm, flip angle = 7°. Signal averaging was performed to yield sufficient signal-to-noise ratio. For signal reception, a flexible 4-channel coil provided by the scanner manufacturer was wrapped around the glass pipe.

Prior to any further WSS analysis, all 2D PC-MR data was checked and corrected for potential phase aliasing. Then, WSS was evaluated at four locations of the pipe cross section (Fig. 1b). The positions of these points, which reflect the position of the boundary, were manually defined in the PC-MR magnitude images. Clauser plot derived WSS values were obtained via a nonlinear regression of the measured data within the logarithmic region (Fig. 1e) which is defined as $6.3 < \ln(\frac{rU_\infty}{\nu}) < 7.1$ according to theory [33]. For each data set, U_∞ was estimated from the mean velocity within a small central region of the pipe flow (Fig. 1b). For comparison, WSS values were also quantified with an in-house developed MATLAB-based software *flow-tool* [5] which essentially uses Eq. (1) for WSS calculation.

Two different data sources were used to obtain reference values for validation of the MR-based Clauser plot derived WSS results: (i) measured data from Laser Doppler Velocimetry (LDV) experiments, and (ii) theoretical WSS values calculated with the so-called friction factor formula [23].

The LDV [34,35] experiments were conducted to provide near-wall velocity measurements with much higher spatial resolution than the MR data. In brief, LDV uses two coherent laser beams focused at a point of interest to create an interference pattern. The flow is seeded with small titanium dioxide particles (~1μm diameter) which scatter the laser light when traveling through the interference pattern. The flow velocity at the point of interest can then be calculated from the frequency of the scatter light intensity oscillations. Cross-sectional velocity information is obtained by successively traversing the interference pattern across

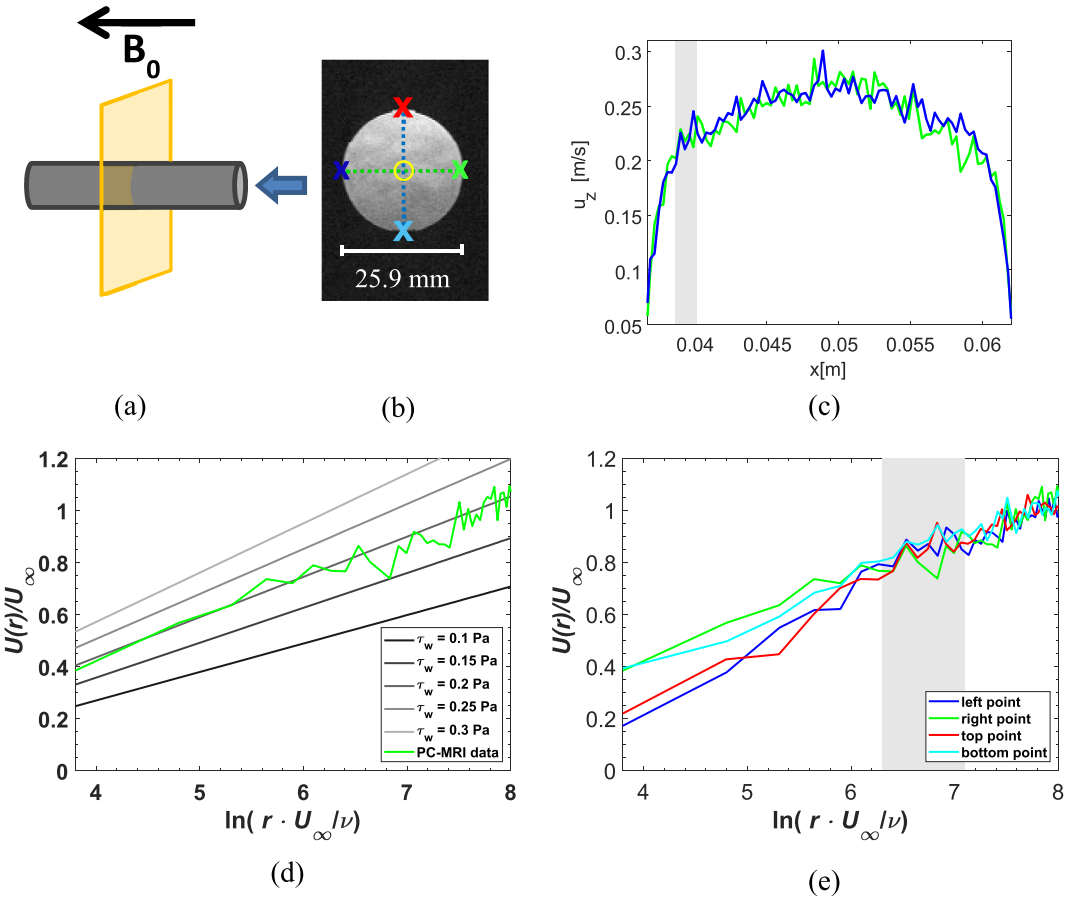

Fig. 1. (a) Experimental setup for flow measurements in glass pipe. (b) Magnitude image of pipe's cross section. The yellow circle indicates the region for estimating the free stream velocity U_∞. (c) Representative velocity profiles along the green and blue dotted lines in (b). (d) Clauser plot for different values of τ_w and measured velocity profile with $Re = 5370$ starting in the right point (green cross in (b)). (e) Clauser plots for the velocity profiles starting at the four positions indicated by color-matched crosses in (b). The shaded area spans the logarithmic region. (For interpretation of the references to color in this figure legend, the reader is referred to the web version of this article.)

the entire pipe cross-section. For these experiments, an LDV system (Flow Explorer, Dantec Dynamics, Skovlunde, Denmark) was operated in backscatter mode with a wavelength of $\lambda = 660$ mm, focal length of $f = 150$ mm and a measurement volume of $331 \times 49 \times 49\ \mu m^3$. LDV velocity measurements were performed under experimental flow conditions identical to the PC-MR measurements for a single Reynolds number of Re = 5370. The LDV velocity profile was captured with a spatial resolution of $\Delta x = 0.0125$ mm. The WSS values were calculated from the LDV profiles identical to PC-MR data via nonlinear regression within the logarithmic region.

In addition, reference WSS values for all experimental Reynolds numbers were calculated using the friction factor formula [23]

$$\tau_w = \frac{1}{8}\lambda\rho v_{\text{mean}}^2 \tag{6}$$

Here, v_{mean} is the measured mean velocity over the entire cross section of the pipe, the constant λ is the so-called Darcy friction factor, which is known from the Moody diagrams [36].

4. Results

Besides the experimental setup, Fig. 1 shows representative velocity profiles as measured with the PC-MR data in fully developed turbulent flow. Further, a representative Clauser plot of a measured velocity profile is given together with theoretical profiles according to the logarithmic law (Eq. (2)) for different values of τ_w.

Fig. 2 summarizes Clauser plots for PC-MR measurements (Re = 5370) with different in-plane resolutions and LDV measurements. The shaded area on Fig. 2 indicates the logarithmic region

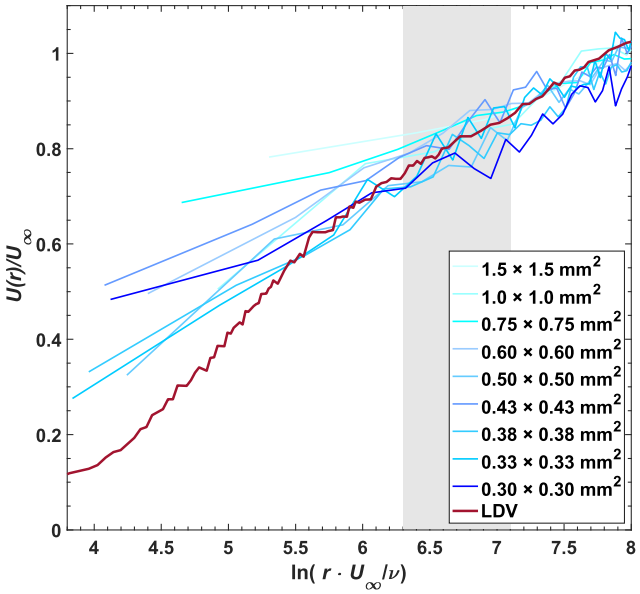

Fig. 2. Representative Clauser plots for measured PC-MR data ($Re = 5370$) with different in-plane resolutions and LDV measurements. The shaded area spans the logarithmic region.

within which the nonlinear regression for WSS estimation was done. The slope $\frac{1}{\kappa}\sqrt{\frac{C_f}{2}}$ of the regression line was computed with reproducible sufficiently low errors (RMSE = 0.03–0.05, R^2 = 0.61–0.85, depending on a point location (Fig. 1b)).

Fig. 3 presents WSS mean values for the three different flow settings as measured with different in-plane resolutions. For comparison, WSS values obtained with the Clauser plot method, the *flow-tool*, and the friction factor formula (Eq. (6)) are illustrated. With increasing Reynolds numbers, larger WSS values were found with an approximately four-fold increase from *Re* = 3000 to 8060. Fig. 3b additionally includes the WSS results from the LDV measurements.

5. Discussion

In this study, the Clauser plot method has been introduced as an alternative approach to evaluate the wall shear stress from PC-MR data. The major advantage of the Clauser method is that it evaluates WSS using the velocity values in the logarithmic region, which is distant from the wall, instead of the velocity derivatives at the wall, where partial volume effects affect velocity measurements. The points very close to the wall are typically the ones which are mostly affected by limited spatial resolution. However, as the signal measured at these points does not enter into computations, the Clauser plot method results are more independent of the underlying spatial resolution.

Overall, the Clauser plots for 2D PC-MR data and LDV measurements were in very good agreement. Deviations were mainly seen in the Clauser plots of the PC-MR data towards smaller values of $\ln(\frac{rU_\infty}{\nu})$ which could be explained by effects from noise and in particular partial volume effects close to the pipe wall.

Moreover, for all Reynolds numbers the extracted WSS values were highly consistent to the reference values based on the friction factor formula (Eq. (6)) (relative deviations ~5%) even for PC-MR data with larger in-plane voxel sizes. This indicates that the Clauser plot method yields correct WSS values in situations when partial volume effects confound velocity measurements in the proximity of the flow boundary.

In contrast, WSS values extracted with the *flow-tool* tend to underestimate the WSS, especially for larger in-plane voxel sizes, i.e. lower spatial resolutions. *Flow-tool* results exhibit a systematic

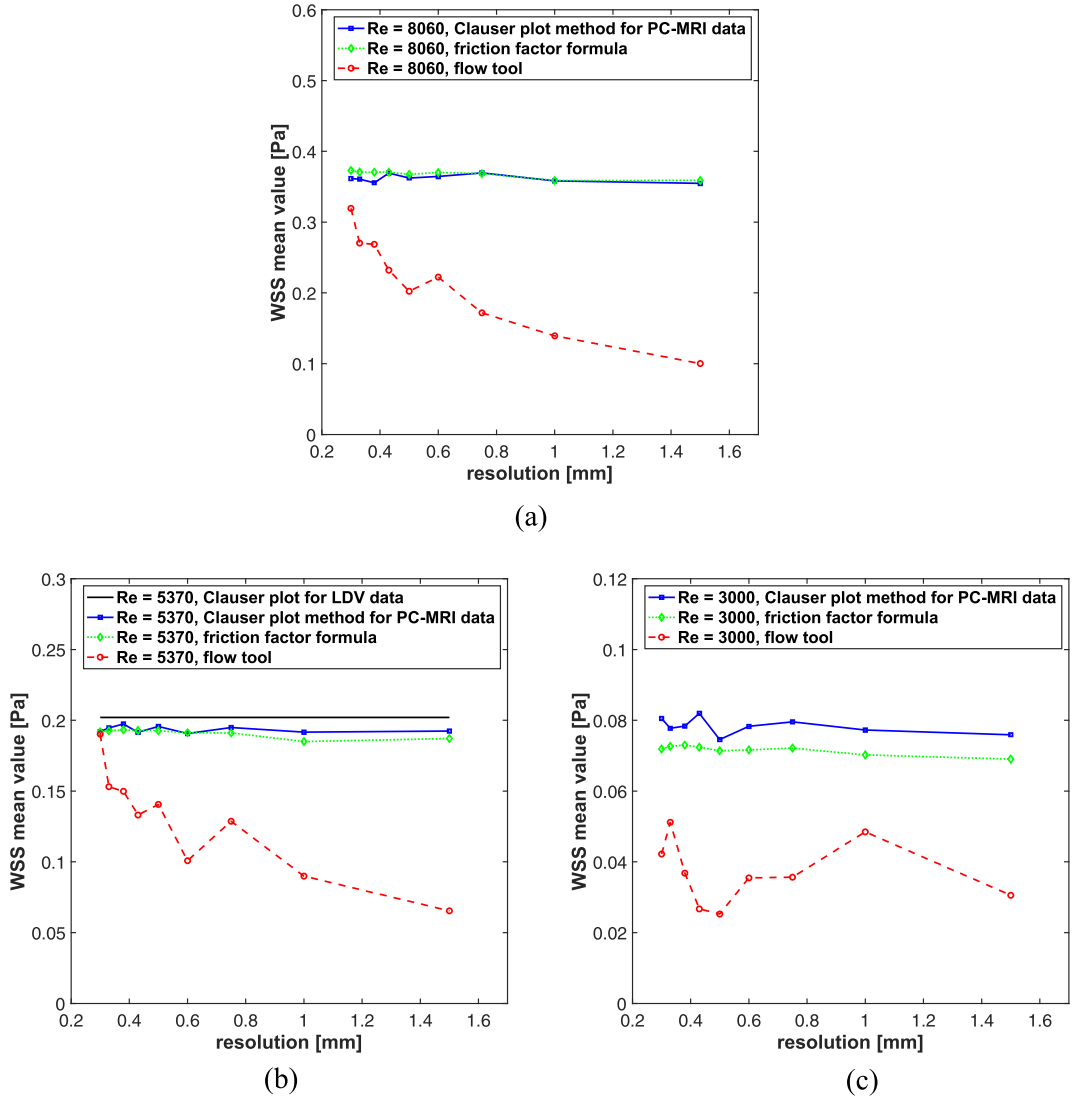

Fig. 3. Results of the MR-derived WSS estimation via the Clauser plot method (solid lines) and *flow-tool* (dashed lines) for Reynolds numbers of (a) 8060, (b) 5370, and (c) 3000, and different in-plane resolutions. In addition, the reference WSS values according to the friction factor formula are given by dotted lines. Results from the LDV measurements at Re = 5370 are illustrated in (b). LDV data was obtained with a single spatial resolution only and is presented as a straight line in (b).

decrease from high to low in-plane showing relative deviations of more than 100%, which could be expected because of partial volume effects. The *flow-tool* currently requires manual segmentation of the wall, which might also cause an additional bias. Although this could be improved, e.g. by automatic segmentation, we believe that this does not play an important role in our experimental evaluation because segmentation of the pipe circular cross section was quite straightforward. The systematic decrease in WSS values obtained with the *flow-tool* is consistent with previous studies on MR-derived WSS estimation [4,5,8,19] which also attribute this behavior to partial volume effects.

Our implementation of the Clauser plot method specifically addresses the problem of limited spatial resolution of PC MRI data. While the limited spatial resolution of the acquired data is the main factor for the variability of PC-MR-derived WSS [3,4,8,19–21], there are also other effects which impact WSS. For example, in [37] it was demonstrated both experimentally and theoretically that higher moments (variance, skewness, kurtosis) of the velocity distribution can severely affect the accuracy of PC velocimetry. This issue could be addressed in further improvements of the WSS estimation.

Due to the fact that the velocities near the boundary of the pipe are substantially smaller compared to the velocities the middle of the pipe, a substantially smaller VENC could be selected to better resolve small velocities close to the boundary. But if the VENC would be too low, then phase aliasing might be too severe so that it could not be properly corrected. Therefore, we have chosen the VENC according to the maximum velocities which occur in the center of the pipe.

A potential limitation of the Clauser plot method for WSS estimation arises from the fact that it was originally designed for fully developed [38] turbulent stationary flows of Newtonian fluids. Blood flow in the aorta is non-stationary pulsatile flow of a non-Newtonian fluid, although blood behaves like a Newtonian fluid in large arteries at high shear rates [25]. However, Computational Fluid Dynamics (CFD) simulations have shown that qualitative flow patterns of Newtonian and non-Newtonian models are similar, but that Newtonian models consistently underestimate the WSS [39]. Although recent research has shown that there might be turbulence in the aortic blood flow, even in healthy subjects [40,41], the assumption of fully developed flow in the aorta is hardly realistic [39] and limited in describing blood flow in vessels [42]. Furthermore, in situations of unsteady turbulent boundary layers, the Clauser plot method should be applied only with great caution [43] without prior knowledge of values of κ and B from the logarithmic law (Eq. (2)). A short investigation of the applicability of the Clauser plot method for *in vivo* blood flow is presented in the Supplementary information. Although the extracted WSS values appear consistent to values reported in literature [21,44], *in vivo* velocity profiles do not follow the logarithmic law. While the results indicate that the Clauser plot method is not applicable to *in vivo* flow, it may nevertheless serve as a valuable validation tool. The application of the method to the data obtained in controllable flow settings may help to check accuracy and reliability of WSS quantification prior to application to *in vivo* data.

In conclusion, the Clauser plot method was shown to be a valuable tool for correct MR-based WSS extraction in fully developed turbulent flow. Although the method is not applicable *in vivo* because of the different flow character, it provides correct WSS values almost independent of the spatial resolution in controllable, stationary flow settings. Therefore, the method renders an alternative approach to obtain MR-based WSS estimates and may serve as helpful approach for validation of MR-based WSS quantification.

Acknowledgements

This study was supported by DFG grant numbers grant numbers DFG HE 1875/30-1, DFG TR 194/56-1, and DFG EG 331/1-1.

Appendix A. Supplementary material

Supplementary data to this article can be found online at https://doi.org/10.1016/j.jmr.2019.05.009.

References

[1] D. Katritsis, L. Kaiktsis, A. Chaniotis, J. Pantos, E.P. Efstathopoulos, V. Marmarelis, Wall shear stress: theoretical considerations and methods of measurement, Spec. Artic. 49 (2007) 307–329, https://doi.org/10.1016/j.pcad.2006.11.001.

[2] M. Markl, A. Frydrychowicz, S. Kozerke, M. Hope, O. Wieben, 4D flow MRI, J. Magn. Reson. Imaging 36 (2012) 1015–1036, https://doi.org/10.1002/jmri.23632.

[3] J. Zimmermann, D. Demedts, H. Mirzaee, P. Ewert, H. Stern, C. Meierhofer, B. Menze, A. Hennemuth, Wall shear stress estimation in the aorta: Impact of wall motion, spatiotemporal resolution, and phase noise, J. Magn. Reson. Imaging 48 (2018) 718–728, https://doi.org/10.1002/jmri.26007.

[4] S. Petersson, P. Dyverfeldt, T. Ebbers, Assessment of the accuracy of MRI wall shear stress estimation using numerical simulations, J. Magn. Reson. Imaging 36 (2012) 128–138, https://doi.org/10.1002/jmri.23610.

[5] A.F. Stalder, M.F. Russe, A. Frydrychowicz, J. Bock, J. Hennig, M. Markl, Quantitative 2D and 3D phase contrast MRI: Optimized analysis of blood flow and vessel wall parameters, Magn. Reson. Med. 60 (2008) 1218–1231, https://doi.org/10.1002/mrm.21778.

[6] W.V. Potters, H.A. Marquering, E. VanBavel, A.J. Nederveen, Measuring wall shear stress using velocity-encoded MRI, Curr. Cardiovasc. Imaging Rep. 7 (2014) 9257, https://doi.org/10.1007/s12410-014-9257-1.

[7] J. Sotelo, L. Dux-Santoy, A. Guala, J. Rodríguez-Palomares, A. Evangelista, C. Sing-Long, J. Urbina, J. Mura, D.E. Hurtado, S. Uribe, 3D axial and circumferential wall shear stress from 4D flow MRI data using a finite element method and a laplacian approach, Magn. Reson. Med. 79 (2018) 2816–2823, https://doi.org/10.1002/mrm.26927.

[8] W.V. Potters, P. Ooij, H. Marquering, E. vanBavel, A.J. Nederveen, Volumetric arterial wall shear stress calculation based on cine phase contrast MRI, J. Magn. Reson. Imaging 41 (2015) 505–516, https://doi.org/10.1002/jmri.24560.

[9] F. Piatti, S. Pirola, M. Bissell, I. Nesteruk, F. Sturla, A. Della Corte, A. Redaelli, E. Votta, Towards the improved quantification of in vivo abnormal wall shear stresses in BAV-affected patients from 4D-flow imaging: Benchmarking and application to real data, Biofluid Mech. Multitude Pathw. Cell. Organ. 50 (2017) 93–101, https://doi.org/10.1016/j.jbiomech.2016.11.044.

[10] E.M. Masutani, F. Contijoch, E. Kyubwa, J. Cheng, M.T. Alley, S. Vasanawala, A. Hsiao, Volumetric segmentation-free method for rapid visualization of vascular wall shear stress using 4D flow MRI, Magn. Reson. Med. 80 (2018) 748–755, https://doi.org/10.1002/mrm.27159.

[11] V.P. Kamphuis, J.J.M. Westenberg, R.L.F. van der Palen, N.A. Blom, A. de Roos, R. van der Geest, M.S.M. Elbaz, A.A.W. Roest, Unravelling cardiovascular disease using four dimensional flow cardiovascular magnetic resonance, Int. J. Cardiovasc. Imaging 33 (2017) 1069–1081, https://doi.org/10.1007/s10554-016-1031-9.

[12] V. Peiffer, S.J. Sherwin, P.D. Weinberg, Does low and oscillatory wall shear stress correlate spatially with early atherosclerosis? A systematic review, Cardiovasc. Res. 99 (2013) 242–250, https://doi.org/10.1093/cvr/cvt044.

[13] A.M. Shaaban, A.J. Duerinckx, Wall shear stress and early atherosclerosis, Am. J. Roentgenol. 174 (2000) 1657–1665, https://doi.org/10.2214/ajr.174.6.1741657.

[14] F. von Knobelsdorff-Brenkenhoff, A. Karunaharamoorthy, R.F. Trauzeddel, A.J. Barker, E. Blaszczyk, M. Markl, J. Schulz-Menger, Evaluation of aortic blood flow and wall shear stress in aortic stenosis and its association with left ventricular remodeling e004038–e004038 Circ. Cardiovasc. Imaging 9 (2016), https://doi.org/10.1161/CIRCIMAGING.115.004038.

[15] P. van Ooij, M. Markl, J.D. Collins, J.C. Carr, C. Rigsby, R.O. Bonow, S.C. Malaisrie, P.M. McCarthy, P.W.M. Fedak, A.J. Barker, Aortic valve stenosis alters expression of regional aortic wall shear stress: New insights from a 4-dimensional flow magnetic resonance imaging study of 571 subjects, J. Am. Heart Assoc. 6 (2017) e005959, https://doi.org/10.1161/JAHA.117.005959.

[16] A. Fatehi Hassanabad, J. Garcia, S. Verma, J.A. White, P.W.M. Fedak, Utilizing wall shear stress as a clinical biomarker for bicuspid valve-associated aortopathy, Curr. Opin. Cardiol. 34 (2019), https://doi.org/10.1097/HCO.0000000000000601.

[17] E.S. Farag, P. van Ooij, R.N. Planken, K.C.P. Dukker, F. de Heer, B.J. Bouma, D. Robbers-Visser, M. Groenink, A.J. Nederveen, B.A.J.M. de Mol, J. Kluin, S.M. Boekholdt, Aortic valve stenosis and aortic diameters determine the extent of increased wall shear stress in bicuspid aortic valve disease, J. Magn. Reson. Imaging 48 (2018) 522–530, https://doi.org/10.1002/jmri.25956.

[18] J. Garcia, A.J. Barker, M. Markl, The role of imaging of flow patterns by 4D flow MRI in aortic stenosis, JACC Cardiovasc. Imaging 12 (2019) 252, https://doi.org/10.1016/j.jcmg.2018.10.034.
[19] C. Montalba, J. Urbina, J. Sotelo, M.E. Andia, C. Tejos, P. Irarrazaval, D.E. Hurtado, I. Valverde, S. Uribe, Variability of 4D flow parameters when subjected to changes in MRI acquisition parameters using a realistic thoracic aortic phantom, Magn. Reson. Med. 79 (2017) 1882–1892, https://doi.org/10.1002/mrm.26834.
[20] P. Dyverfeldt, M. Bissell, A.J. Barker, A.F. Bolger, C.-J. Carlhäll, T. Ebbers, C.J. Francios, A. Frydrychowicz, J. Geiger, D. Giese, M.D. Hope, P.J. Kilner, S. Kozerke, S. Myerson, S. Neubauer, O. Wieben, M. Markl, 4D flow cardiovascular magnetic resonance consensus statement, J. Cardiovasc. Magn. Reson. 17 (2015) 72, https://doi.org/10.1186/s12968-015-0174-5.
[21] F.M. Callaghan, S.M. Grieve, Normal patterns of thoracic aortic wall shear stress measured using four-dimensional flow MRI in a large population, Am. J. Physiol.-Heart Circ. Physiol. 315 (2018) H1174–H1181, https://doi.org/10.1152/ajpheart.00017.2018.
[22] F.H. Clauser, The turbulent boundary layer, in: H.L. Dryden, T. von Kármán (Eds.), Adv. Appl. Mech., Elsevier, 1956, pp. 1–51. https://doi.org/10.1016/S0065-2156(08)70370-3.
[23] H. Schlichting, K. Gersten, Boundary-layer Theory, nineth ed., Springer-Verlag, Berlin Heidelberg, 2017.
[24] F. Irgens, Rheology and Non-Newtonian Fluids, first ed.,, Springer International Publishing, 2014.
[25] K.B. Chandran, S.E. Rittgers, A.P. Yoganathan, Biofluid Mechanics: the Human Circulation, second ed., CRC Press, 2012.
[26] C. Tropea, A. Yarin, J.F. Foss (Eds.), Springer Handbook on Experimental Fluid Mechanics, first ed., Springer-Verlag, Berlin Heidelberg, 2007.
[27] S.C.C. Bailey, M. Vallikivi, M. Hultmark, A.J. Smits, Estimating the value of von Kármán's constant in turbulent pipe flow, J. Fluid Mech. 749 (2014) 79–98, https://doi.org/10.1017/jfm.2014.208.
[28] K.T. Trinh, On the Karman constant. Eprint ArXiv10070605 2010: arXiv:1007.0605.
[29] E.-S. Zanoun, F. Durst, H. Nagib, Evaluating the law of the wall in two-dimensional fully developed turbulent channel flows, Phys. Fluids 15 (2003) 3079–3089, https://doi.org/10.1063/1.1608010.
[30] G.K. El Khoury, P. Schlatter, A. Noorani, P.F. Fischer, G. Brethouwer, A.V. Johansson, Direct numerical simulation of turbulent pipe flow at moderately high Reynolds numbers, Flow Turbul. Combust. 91 (2013) 475–495, https://doi.org/10.1007/s10494-013-9482-8.
[31] T. Wei, R. Schmidt, P. McMurtry, Comment on the Clauser chart method for determining the friction velocity, Exp. Fluids. 38 (2005) 695–699, https://doi.org/10.1007/s00348-005-0934-3.
[32] J.F. Schenck, The role of magnetic susceptibility in magnetic resonance imaging: MRI magnetic compatibility of the first and second kinds, Med. Phys. 23 (1996) 815–850, https://doi.org/10.1118/1.597854.
[33] S.B. Pope, Turbulent flows, Cambridge University Press, 2000.
[34] F. Durst, A. Melling, J.H. Whitelaw, Principles and Practice of Laser Doppler Anemometry, Academic Press, 1976.
[35] H.-E. Albrecht, N. Damaschke, M. Borys, C. Tropea, Laser Doppler and Phase Doppler Measurement Techniques, Springer-Verlag, Berlin Heidelberg, 2003.
[36] L.F. Moody, Friction factors for pipe flows, Trans. Am. Soc. Mech. Eng. 66 (1944) 671–678.
[37] A. Vallatos, H.F.I. Al-Mubarak, J.M. Mullin, W.M. Holmes, Accuracy of phase-contrast velocimetry in systems with skewed intravoxel velocity distributions, J. Magn. Reson. 296 (2018) 121–129, https://doi.org/10.1016/j.jmr.2018.09.002.
[38] Y.A. Çengel, J.M. Cimbala, Fluid Mechanics: Fundamentals and Applications, fourth ed.,, McGraw-Hill Education, 2018.
[39] S. Madhavan, E.M.C. Kemmerling, The effect of inlet and outlet boundary conditions in image-based CFD modeling of aortic flow, Biomed. Eng. Online 17 (2018) 66–166, https://doi.org/10.1186/s12938-018-0497-1.
[40] H. Ha, M. Ziegler, M. Welander, N. Bjarnegård, C.-J. Carlhäll, M. Lindenberger, T. Länne, T. Ebbers, P. Dyverfeldt, Age-related vascular changes affect turbulence in aortic blood flow, Front. Physiol. 9 (2018) 36–136, https://doi.org/10.3389/fphys.2018.00036.
[41] L. Prahl Wittberg, S. van Wyk, L. Fuchs, E. Gutmark, P. Backeljauw, I. Gutmark-Little, Effects of aortic irregularities on blood flow, Biomech. Model. Mechanobiol. 15 (2016) 345–360, https://doi.org/10.1007/s10237-015-0692-y.
[42] P.S. Ayyaswamy, Chapter 16 - Introduction to biofluid mechanics, in: P.K. Kundu, I.M. Cohen, D.R. Dowling (Eds.), Fluid Mech., sixth ed., Academic Press, 2016: pp. e1–e73.
[43] G.J. Brereton, Deduction of skin friction by Clauser technique in unsteady turbulent boundary layers, Exp. Fluids 7 (1989) 422–424, https://doi.org/10.1007/BF00193426.
[44] R.L.F. van der Palen, A.A.W. Roest, P.J. van den Boogaard, A. de Roos, N.A. Blom, J.J.M. Westenberg, Scan-rescan reproducibility of segmental aortic wall shear stress as assessed by phase-specific segmentation with 4D flow MRI in healthy volunteers, Magma N. Y. N. 31 (2018) 653–663, https://doi.org/10.1007/s10334-018-0688-6.